ACCEPTED VERSION

Can Wang, An Deng, Abbas Taheri, Honghua Zhao, Jie Li

Modelling particle kinetic behaviour considering asperity contact: formulation and DEM simulations

Granular Matter, 2019; 21(2):1-16

© Springer-Verlag GmbH Germany, part of Springer Nature 2019

This is a post-peer-review, pre-copyedit version of an article published ***in*** *Granular Matter****.*** *The final authenticated version is available online at: http://dx.doi.org/10.1007/s10035-019-0879-5*

PERMISSIONS

https://www.springer.com/gp/open-access/publication-policies/self-archiving-policy

Self-archiving for articles in subscription-based journals

Springer journals' policy on preprint sharing.

By signing the Copyright Transfer Statement you still retain substantial rights, such as self-archiving:

Author(s) are permitted to self-archive a pre-print and an author's accepted manuscript version of their Article.
……….

b. An Author's Accepted Manuscript (AAM) is the version accepted for publication in a journal following peer review but prior to copyediting and typesetting that can be made available under the following conditions:

(i) Author(s) retain the right to make an AAM of their Article available on their own personal, self-maintained website immediately on acceptance,

(ii) Author(s) retain the right to make an AAM of their Article available for public release on any of the following 12 months after first publication ("Embargo Period"): their employer's internal website; their institutional and/or funder repositories. AAMs may also be deposited in such repositories immediately on acceptance, provided that they are not made publicly available until after the Embargo Period.

An acknowledgement in the following form should be included, together with a link to the published version on the publisher's website: "This is a post-peer-review, pre-copyedit version of an article published in [insert journal title]. The final authenticated version is available online at: http://dx.doi.org/[insert DOI]".

When publishing an article in a subscription journal, without open access, authors sign the Copyright Transfer Statement (CTS) which also details Springer's self-archiving policy.

See Springer Nature terms of reuse for archived author accepted manuscripts (AAMs) of subscription articles.

11 June 2020

http://hdl.handle.net/2440/119576

Modelling particle kinetic behaviour considering asperity contact: Formulation and DEM simulations

Can Wang[1], An Deng[1*], Abbas Taheri[1], Honghua Zhao[2], Jie Li[3]

[1] School of Civil, Environmental and Mining Engineering, The University of Adelaide, SA 5005, Australia.

[2] State Key Laboratory of Structural Analysis for Industrial Equipment, Department of Engineering Mechanics, Dalian University of Technology, Dalian, Liaoning 116023, China

[3] School of Civil and Infrastructure Engineering, RMIT University, VIC 3001, Australia.

[*] Corresponding author: an.deng@adelaide.edu.au.

Abstract

A model of formulating particle kinetic behaviour considering surface asperity is presented. The asperity was created by lining up on the surface a set of particles in varying distances. A moving particle was assigned a velocity to travel on the rugged surface where the particle trajectory and mechanical energy were gauged. The results were used to validate a discrete element framework which was developed and applied to examine the effect of surface asperity on the particle kinetic behaviour. Some interesting case studies were designed and simulated. The simulations suggested that the surface roughness influenced the energy dissipation caused in the particle–surface collisions. The research outcomes defined the inter-particle reaction from a micro-scale perspective and helped predict asperity-induced wear.

Keywords: surface roughness, collision, contact mechanics, energy dissipation

1. Introduction

Upon contacting, particles behaviour is closely dependent on its physical characteristics, such as the density, shape, size and surface at contact [1-3]. On the contact surface, the asperity, or roughness, governs the particle response, mainly in the form of energy loss in a dynamic or tribological process (e.g., the wheel rolling on the rail) [4-7]. The energy loss, at least a major portion of it, is recognised of arising from the surface adhesion and frictional properties [6-8]. This means that the energy loss in itself is caused primarily by the surface deformation at contact. According to Buckley [9], the deformation includes the elastic and plastic components. The two components are related to the conditions of contact existed between the particles of concern and, depending on the contact conditions, are subject to variation in magnitude. As a result, the relationship between the surface asperity, deformation components, and energy loss is still poorly understood [10-11]. Albeit there are experimental solutions (e.g. [3,9]) developed to eliminate the lack of understanding, the test conditions are less than ideal, and the corresponding results are not accurate enough. The reasons, as per Zappone et al. [12], were the challenge to set up a well-defined rough surface and the difficulty to avoid environmental noises (e.g., the surface chemistry characteristics) surrounding the particles in the test. These difficulties can be resolved through mathematical tools which enable a virtual system free of environmental disturbance.

In this study, a discrete element model (DEM) was developed to reproduce the system and approximate particle kinetic behaviour in response to the surface asperity that the particle is subjected to. The surface asperity characteristics were defined specifically to subject the particle to a unique, exclusive rugged surface. On the rugged surface, the particle was assigned a velocity and allowed to travel through. The model was used to gauge the particle trajectory and velocity in travel so that the energy loss was recorded. The model was validated against the analytical solution established in the same asperity conditions as for the DEM model. DEM simulations were performed on some interesting case studies in order to gain a further insight into the particle kinetic behaviour at micro-scale.

2. Model Development

2.1 Geometry

The geometry used to develop the model is provided in Figure 1. An array of semicircular discs, 1 to N, are lined up at fixed positions in (x, y) plane, forming the asperity based on the substrate of x-axis. The discs are equal in radius, r_j, where j=1, 2,…, N, and placed edge to edge with individual centroids sitting on the x-axis. At time t, disc M moves at a velocity, v, in the x-direction. Disc M measures r in radius and m in mass. The position of the moving disc in relation to disc j is determined by the contact angle, γ, which measures the angle from the x-axis to the centre-to-centre line drawn between discs M and j. Disc M is in contact with disc j at point A. This model uses circular asperities (which are less angular than some surface projections), but as suggested in past studies [13-15], this geometry defines a clear, continuous and manageable asperity surface. This geometry facilitates: *i*) the expression of the asperity surface (i.e. circular function), *ii*) the assessment of discs contacting condition, and *iii*) the adaption of the geometry to the analytical model [16]. Similar circular, spaced asperities were adopted in past studies [14-15,17-19]. The model geometry in the current study however differs in the following aspects: *i*) the substrate being horizontal thus avoiding the angle of inclination, *ii*) the substrate being fixed, and *iii*) the single disc moving through the asperity. In addition, we assumed the following conditions: *i*) There is no sub-asperity at the particle surface; *ii*) the discs and surface are smooth and, as per Gollin et al. [20], the energy loss is in the form of collisional energy dissipation; and *iii*) the collisions are elasto-viscous. In this current study, the collisional energy dissipation was determined using two approaches: the discrete element simulation method and the analytical solution. The analytical results were used to verify the simulation results. The two approaches and the method verification are presented in the following sections.

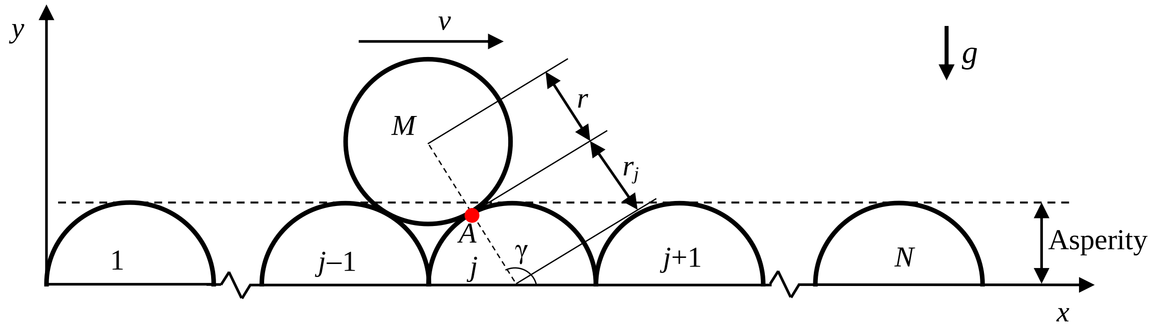

Figure 1. The model geometry of disc *M* moving at velocity *v* on the asperity surface, a substrate comprised of an array of equal-size semi-discs 1 to *N* which are arranged, edge-to-edge, with respective centroids sitting on *x*-axis.

2.2 DEM model

The DEM model was developed to reproduce the mechanical responses of two or more discs at contact, e.g., point *A* in Figure 1. As per Cundall [21], the mechanical responses at contact can be represented by using a combination of simple mechanical elements, such as the spring, slider and dashpot. The combination is dependent on the materials to be examined and, as suggested in the past similar studies [17-19,22], is often governed by the Hertz Contact model [23]. The Hertz Contact model uses the least number of mechanical elements, as illustrated in Figure 2, but enables the mimicking of a wide range of distinct element based problems. The model is simple in concept and preferably applicable to represent the contacting occurred between the kinetic particles.

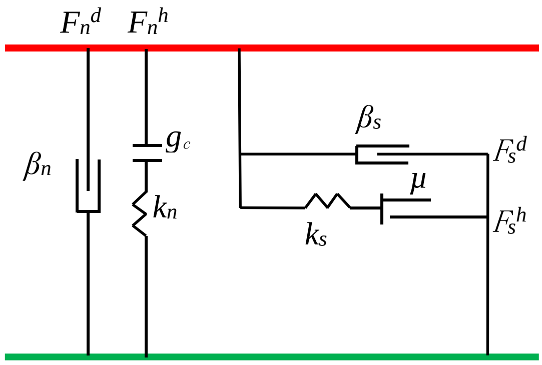

Figure 2. Diagram of the Hertz Contact model (adapted from ITASCA [24]), where F_n^h and F_s^h are respectively non-linear contact force at normal and shear direction; F_n^d and F_s^d are dashpot (viscous) forces at normal and shear direction, respectively; β_n and β_s are damping coefficients at normal and shear direction, respectively; k_n and k_s are stiffness at normal and shear direction, respectively; g_c is gap distance between the two bodies of interest; and μ is friction coefficient.

In the Hertz Contact model, the individual mechanical elements govern energy transformation occurred at particles contact. The energy transformation arises from three components: the elastic strain energy, E_s, stored in the spring elements, the slip energy, E_μ, dissipated by frictional sliding, and the dashpot energy, E_β, being dissipated due to damping [25]. The energy is dissipated to other forms of energy, e.g., heat and sound. Owning to the no-friction contact as defined in Figure 1, the dashpot energy dissipation E_β is the only source of energy loss at contact. For the same reason, the moving disc M changes only its normal velocity component [26]. The energy loss E_β is expressed as:

$$E_\beta = -\sum F_n^d \left(\dot{\delta}_n \Delta t \right) \tag{1}$$

where δ_n is the relative normal displacement; Δt is the time step increment; F_n^d is the normal dashpot force at contact and, as per Itasca [24], is calculated as:

$$F_n^d = 2\dot{\delta}_n^2 \beta_n \sqrt{m_c k_n} \tag{2}$$

where β_n is the normal critical damping coefficient, k_n is the normal stiffness, and m_c is the mass of the system of interest and defined by:

$$m_c = \frac{m_1 m_2}{m_1 + m_2} \tag{3}$$

where m_1 and m_2 are the mass of discs 1 and 2 respectively.

In a DEM model, the particles are assumed to be non-deformable. Instead an overlap is allowed to develop at the point of contact in order to account for disc-to-disc interactions [25]. This overlap likely influences the trajectory of the moving disc, as illustrated in Figure 3. Figure 3 shows the potential overlap at the contact between moving disc *P* and stationary disc *Q*. The two discs collide at an eccentricity of *L*. DEM algorithm allows disc *P* to penetrate into disc *Q*, creating a contact overlap as shaded between the two discs. As a result, the centroid of disc *P* passes on the trajectory of points *A*, *B* and *C* in DEM simulation, but in reality may not pass through point *B*. The influence to the trajectory of disc *P* may be negligible in one collision. However, where a continuously bumpy surface as in Figure 1 is of the choice and multiple collisions occur, the influences may accumulate, likely leading to noticeable trajectory deviation. The change in trajectory is supposed to affect the prediction of the contact angle γ which in turn brings possible inaccuracy to estimate of the energy loss of the moving disc. The overlap influence can be examined by cross checking the simulation results with the results obtained from an analytical solution.

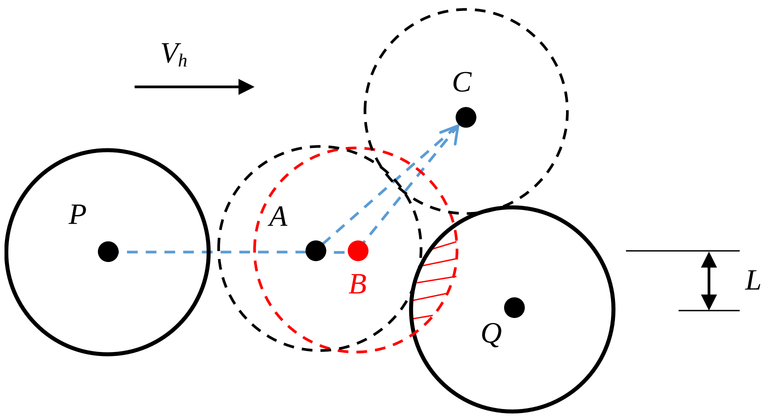

Figure 3. The centroid of particle *P* travelling, at velocity v_h, in trajectory of A–B–C occurred during an oblique collision with particle *Q*.

2.3 Analytical solution

This section presents the analytical solution to the same problem of the disc travelling on asperity surface as simulated by the DEM approach. The DEM adopts the Newton's laws of motion, and the analytical solution considers the restitution of material. According to [22,26], both the Newton's laws of motion and the restitution can be used to describe the dissipative interaction of particles. As per Doménech-Carbó [4] and Ling [27], the restitution coefficient quantifies the elastic energy restored at contact, which is recovered back to kinetic energy, and the energy dissipation that results from plastic deformation. Upon surface colliding, no body penetration (i.e., the overlap) between the discs of interest is allowed. Therefore, the analytical method offers an accurate prediction of the disc trajectory and can be used to examine the influences of overlap identified in the DEM simulation.

2.3.1 Model description

The geometry in Figure 1 was adapted to the geometry in Figure 4. The new element added is the centroid profile where the centroid of disc *M* lies on. The profile was plotted based on the radii of the discs so that the overlap issue was avoided. On the centroid profile, a sub-profile, curve *BC*, was plotted to illustrate one disc bounce. Multiple bounces may occur depending on the kinetic energy of the moving disc and the disc material properties assigned. The rest conditions such as the surface asperity, velocity and radii remained the same as in Figure 1. When disc *M* moved on the bumpy surface, the following conditions were assumed: *i*) Only the point of contact was examined during the collision; and *ii*) Disc collision completed instantaneously, so that the collision time was negligible. These conditions were used to simplify the model and to agree with the conditions assumed for the DEM approximation.

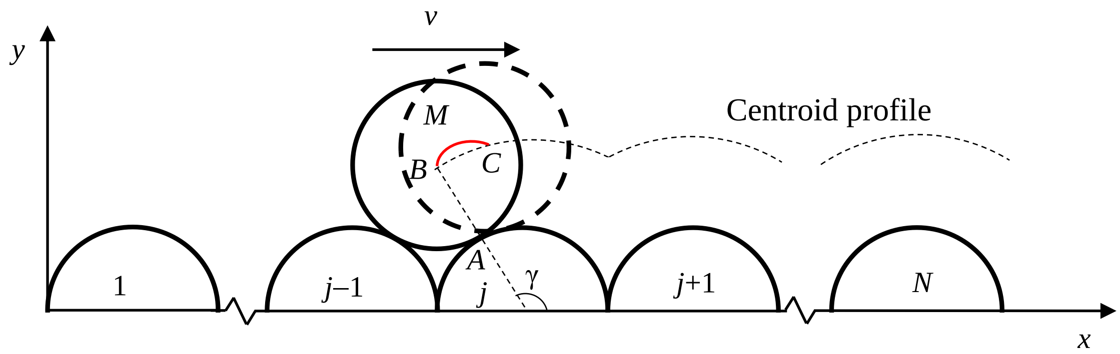

Figure 4. The model geometry of disc *M* moving, with the consideration of bounces, at velocity *v* on the asperity surface which is comprised of an array of equal-size semi-discs 1 to *N* arranged, edge-to-edge, with centroids sitting on *x*-axis.

At a moment when disc *M* travels on the asperity surface, the disc takes one of three moves: rotating, sliding and bouncing. As there is no surface friction, the disc does not spin. Therefore the disc either slides or bounces on the surface, depending on the condition of contact between the moving disc and one of the base discs. The contact condition can be judged based on the centre-to-centre distance D_j^t measured at time *t* between discs *M* and *j*, which is expressed as

$$D_j^t = \sqrt{\left(x^t - x_j\right)^2 + \left(y^t - y_j\right)^2} \tag{4}$$

where (x_j, y_j) and (x^t, y^t) are the coordinates of the centres of discs *j* and *M*, respectively. Disc *M* is bouncing if $D_j^t > r + r_j$ or sliding if $D_j^t = r + r_j$. The condition $D_j^t < r + r_j$ is not allowed to avoid the surface overlap. For base disc *j*, the centre coordinate is expressed as:

$$x_j = r_j + 2\sum_{i=1}^{j-1} r_i \tag{5}$$

$$y_j = 0 \tag{6}$$

2.3.2 Trajectory of bouncing

Upon a collision with disc *j*, disc *M* loses a portion of the normal velocity. The residual normal velocity drives the disc to bounce up and then falls under gravity, as of the profile *BC* shown in Figure 4. This bouncing process continues several times until the normal velocity vanishes. Assume disc *M* is in collision with disc *j* at time *t*. Meanwhile, the disc bounces up at velocity components (v_x^t , v_y^t). If, at time step t+Δt, disc *M* is in the move of the first bounce, the corresponding velocity components become:

$$v_x^{t+\Delta t} = v_x^t \tag{7}$$

$$v_y^{t+\Delta t} = v_y^t + g \times \Delta t \tag{8}$$

The centr relocates to location ($x^{t+\Delta t}$, $y^{t+\Delta t}$) which are respectively expressed as:

$$x^{t+\Delta t} = x^t + v_x^t \times \Delta t \tag{9}$$

$$y^{t+\Delta t} = y^t + \frac{\left(v_y^{t+\Delta t} + v_y^t\right) \times \Delta t}{2} \tag{10}$$

Substitute Eqs. (9) and (10) to Eq. (4) to update discs centre-to-centre distance $D_j^{t+\Delta t}$. The updated $D_j^{t+\Delta t}$ is then used to confirm the occurrence of the first bounce presemted for disc *M*. If $D_j^{t+\Delta t} > r + r_j$ the presumption is confirmed; if $D_j^{t+\Delta t} = r + r_j$, the disc is sliding; and if $D_j^{t+\Delta t} < r + r_j$, disc *M* has performed two or more bounces in the time step increment Δt.

Where two or more bounces occur in the time step increment Δt, the time $t+\Delta t_0$ when the first bounce completes needs to be determined. As Δt is sufficiently small (and Δt_0 is further smaller), the horizontal and vertical velocities are assumed to be constant during the collision period Δt_0. Assuming a linear trajectory during (t, $t+\Delta t_0$), the centre of disc M, ($x^{t+\Delta t_0}$, $y^{t+\Delta t_0}$), satisfies the translation condition:

$$y^{t+\Delta t_0} = y^t + \frac{v_y^{t+\Delta t_0}}{v_x^{t+\Delta t_0}} x^{t+\Delta t_0} - \frac{v_y^{t+\Delta t_0}}{v_x^{t+\Delta t_0}} x^t \tag{11}$$

At time $t+\Delta t_0$, discs M and j are in contact, leading to

$$\left(y^{t+\Delta t_0}\right)^2 + \left(x^{t+\Delta t_0} - x_j\right)^2 = \left(r + r_j\right)^2 \tag{12}$$

Solving Eqs. (11) and (12) yields two roots $x^{t+\Delta t_0} = x_1$ and x_2 respectively as follow:

$$x^{t+\Delta t_0} = \begin{cases} x_1, \text{ if } \left|x_1 - x^t\right| < \left|x_2 - x^t\right| \\ x_2, \text{ if } \left|x_1 - x^t\right| > \left|x_2 - x^t\right| \end{cases} \tag{13}$$

The time increment Δt_0 is calculated as:

$$\Delta t_0 = \left|\frac{x^{t+\Delta t_0} - x^t}{v_x^t}\right| \tag{14}$$

During the time increment Δt_0, the x-velocity component of disc M remains unchanged:

$$v_x^{t+\Delta t_0} = v_x^t \tag{15}$$

Disc M changes in elevation, the y-velocity component is updated as:

$$v_y^{t+\Delta t_0} = \lim_{\Delta t_0 \to 0} \frac{v_y^t}{\left|v_y^t\right|} \sqrt{\left(v_y^t\right)^2 - 2g\left(y^t - y^{t+\Delta t_0}\right)} \tag{16}$$

The contact angle γ at $t+\Delta t_0$ becomes:

$$\gamma^{t+\Delta t_0} = \arctan \frac{y^{t+\Delta t_0} - y_j}{x^{t+\Delta t_0} - x_j} \tag{17}$$

The tangential and normal velocity components are calculated respectively as:

$$v_s^{t+\Delta t_0} = v_x^{t+\Delta t_0} \cos \gamma^{t+\Delta t_0} + v_y^{t+\Delta t_0} \sin \gamma^{t+\Delta t_0} \tag{18}$$

$$v_n^{t+\Delta t_0} = v_x^{t+\Delta t_0} \sin \gamma^{t+\Delta t_0} + v_y^{t+\Delta t_0} \cos \gamma^{t+\Delta t_0} \tag{19}$$

If the disc rebounds, the disc is subjected to damping and the normal velocity reduces to:

$$v_{n,r}^{t+\Delta t_0} = -\alpha_n v_n^{t+\Delta t_0} \tag{20}$$

where α_n is the material restitution coefficient. Kawaguchi et al. [28] expressed α_n as a function of damping coefficient β_n:

$$\alpha_n = e^{\frac{\beta_n \pi}{\sqrt{1-\beta_n^2}}} \tag{21}$$

Substituting Eq. (21) into Eq. (20) yields:

$$v_{n,r}^{t+\Delta t_0} = -e^{\frac{\beta_n \pi}{\sqrt{1-\beta_n^2}}} v_n^{t+\Delta t_0} \tag{22}$$

Transforming the tangential and normal velocity components to velocity components in (x, y) plane, we have:

$$v_x^{t+\Delta t_0} = v_s^{t+\Delta t_0} \cos\gamma - v_{n,d}^{t+\Delta t_0} \sin\gamma \tag{23}$$

$$v_y^{t+\Delta t_0} = v_s^{t+\Delta t_0} \sin\gamma - v_{n,d}^{t+\Delta t_0} \cos\gamma \tag{24}$$

The new velocity components drive the disc to rebound. At time step $t+\Delta t$, the velocity of disc M and the coordinate of the centre are determined respectively as:

$$v_x^{t+\Delta t} = v_x^{t+\Delta t_0} \tag{25}$$

$$v_y^{t+\Delta t} = v_y^{t+\Delta t_0} + g\left(\Delta t - \Delta t_0\right) \tag{26}$$

$$x^{t+\Delta t} = x^{t+\Delta t_0} + v_x^{t+\Delta t_0}\left(\Delta t - \Delta t_0\right) \tag{27}$$

$$y^{t+\Delta t} = y^{t+\Delta t_0} + v_y^{t+\Delta t_0}\left(\Delta t - \Delta t_0\right) \tag{28}$$

The coordinate of the discs centre is subject to the contact criterion (i.e. $D_j^{t+\Delta t}$ *vs.* $r + r_j$). If $D_j^{t+\Delta t} > r + r_j$, disc M is in the move of the second bounce. The algorithm proceeds to the next time step. Otherwise, Eqs. (11)–(28) are skipped and the current bounce completes, and the disc enters into the phase of sliding. The skipping is acceptable as the normal velocity at $t+\Delta t_0$ is sufficiently small and in period ($t+\Delta t_0$, $t+\Delta t$) the remaining bounces are relatively small in scale and less in number, and are negligible. The neglected trivial bounces would influence the determination of kinetic energy loss of disc *M* and thus its trajectory. However, the influence is very small if not zero because time step increment Δt itself is a significantly small value, i.e., $\times 10^{-4}$ s, and a smaller value for increment $\Delta t - \Delta t_0$, e.g., $\times 10^{-6}$ s, causes marginal changes to the trajectory.

2.3.3 Trajectory of sliding

Where the normal velocity of disc *M* dissipates completely at time $t+\Delta t_0$, the disc does not bounce but enters into sliding on the surface. Upon departure, the angular velocity is determined as:

$$\omega^{t+\Delta t_0} = \frac{v_s^{t+\Delta t_0}}{r + r_j} \tag{29}$$

where the tangential velocity $v_s^{t+\Delta t_0}$ is determined in terms of Eq. (18). Meanwhile, the angular acceleration $\omega^{t+\Delta t_0}$ is equal to:

$$\dot{\omega}^{t+\Delta t_0} = \frac{g \times \cos \gamma^{t+\Delta t_0}}{r + r_j} \tag{30}$$

The angle of rotation θ completed during the time increment $(\Delta t - \Delta t_0)$ is calculated as:

$$\theta^{t+\Delta t_0, t+\Delta t} = \omega^{t+\Delta t_0} \times \left(\Delta t - \Delta t_0\right) + 0.5 \times \omega^{t+\Delta t_0} \times \left(\Delta t - \Delta t_0\right)^2 \tag{31}$$

Define angles θ and γ to be positive if they rotate in clockwise and anti-clockwise directions respectively, as shown in Figure 5.

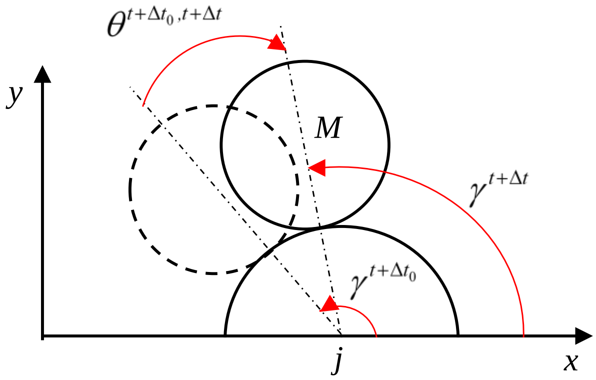

Figure 5. The schematic of the change of the contact angle γ and rotation angle θ occurred at time increment $t+\Delta t_0$ to $t+\Delta t$ when the moving disc *M* slides on the base disc *j*.

At time step $t+\Delta t$, the contact angle is updated as:

$$\gamma^{t+\Delta t} = \gamma^{t+\Delta t_0} - \theta^{t+\Delta t_0, t+\Delta t} \tag{32}$$

The centre of disc *M* relocates to:

$$x^{t+\Delta t} = x^{t+\Delta t_0} + \left(r + r_j\right) \times \left(\cos\left(\gamma^{t+\Delta t_0} - \theta^{t+\Delta t_0, t+\Delta t}\right) - \cos\gamma^{t+\Delta t_0}\right) \tag{33}$$

$$y^{t+\Delta t} = y^{t+\Delta t_0} + \left(r + r_j\right) \times \left(\sin\left(\gamma^{t+\Delta t_0} - \theta^{t+\Delta t_0, t+\Delta t}\right) - \sin\gamma^{t+\Delta t_0}\right) \tag{34}$$

The angular velocity ω, tangential velocity v_s, *x*-velocity component v_x, and *y*-velocity component v_y, respectively, are updated as:

$$\omega^{t+\Delta t} = \frac{\omega^t}{\left|\omega^t\right|} \times \sqrt{\left(\omega^t\right)^2 - 2 \times g \times \frac{y^{t+\Delta t} - y^t}{\left(r + r_j\right)^2}} \tag{35}$$

$$v_s^{t+\Delta t} = \omega^{t+\Delta t} \times \left(r + r_j\right) \tag{36}$$

$$v_x^{t+\Delta t} = v_s^{t+\Delta t} \times \cos\left(\gamma^{t+\Delta t}\right) \tag{37}$$

$$v_y^{t+\Delta t} = v_s^{t+\Delta t} \times \sin\left(\gamma^{t+\Delta t}\right) \tag{38}$$

Eqs. (29)–(38) are used to calculate the trajectory of disc *M* performed during time step ($t+\Delta t_0$, $t+\Delta t$). Continue the same algorithm at the next time increment ($t+\Delta t$, $t+2\Delta t$) if disc *M* is sliding in terms of the contact criterion of $D_j^{t+2\Delta t}$ *vs.* $r+r_j$. Otherwise, the algorithm developed for bouncing, i.e. Eqs. (11)–(28), is used. An additional contact check is performed between discs *M* and *j*+1. If, at time *t*, $x^t > x_j + r_j$, then disc *M* is in contact with disc *j*+1 and disc *j*+1 becomes the current disc of interest in the algorithm.

2.3.4 Model flowchart

A flowchart of the model is presented in Figure 6. The initial input values include the velocity components and the position of the centre of disc *M*. The position values are plugged in the contact criterion of D_j^t *vs.* $r+r_j$ to determine the motion of the disc. Where in the motion of bouncing, disc *M* is updated, using the corresponding algorithm, in respect to its centre coordinate and velocity components. The new values are subject to the contact criterion again. Where disc *M* is in the motion of sliding, the new values are plugged into the algorithm for sliding, thus updating the centre position and disc velocity. And the new values flow to the contact criterion again. In either motion, disc *M* is subject to the check of contact with the next base disc *j*+1. If there is, disc *j*+1 becomes the current base disc, and a new loop runs. Before the flowchart ends, the *x*-velocity component is checked. If the velocity component is not equal to zero, the loop keeps on running. Otherwise, the program ends.

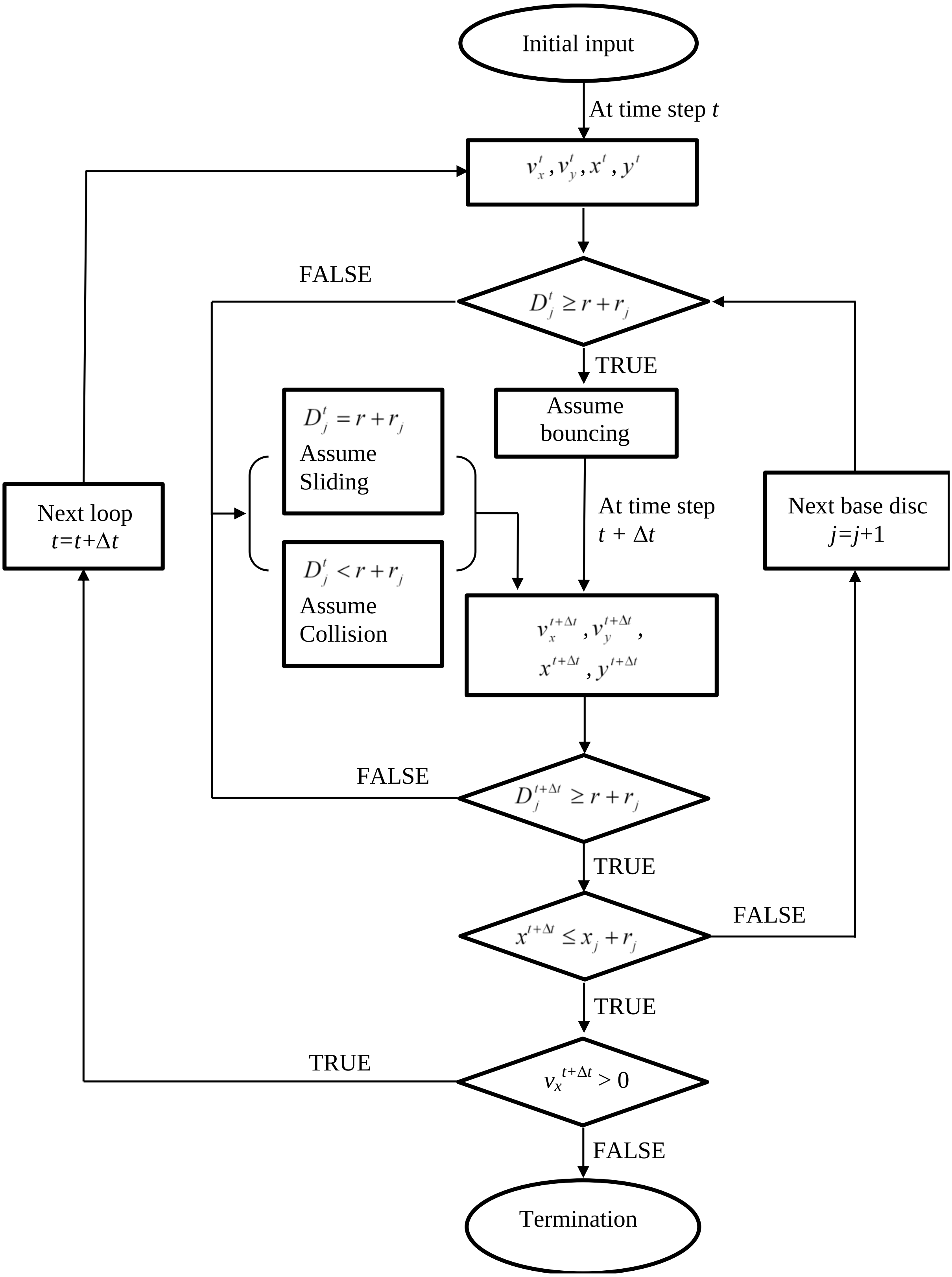

Figure 6. Computer flowchart developed to guide the travel of the moving disc on a bumpy surface.

3. DEM Validation

The DEM model was validated against the analytical solution. Both approaches were applied to the model shown in Figure 1. The models were established using the following properties. The radii were 0.3 m for the moving disc and 0.05 m for the base disc. All discs had a density of 2,000 kg/m³. In the DEM, the Hertz contact was used which adopted a Poisson's ratio of 0.3 and shear modulus of 100 GPa. The relatively large shear modulus was assumed to reduce the influence of the contact overlap, enabling a simulation environment similar to that for the analytical method. For both methods, a damping coefficient β_n = 0.5 was used to dissipate energy at each collision. The moving disc was assigned three initial velocities v_x^0 = 0.3, 0.5 and 1.0 m/s respectively. The results of the horizontal velocity versus the distance for the disc assigned the three initial velocities are provided in Figure 7.

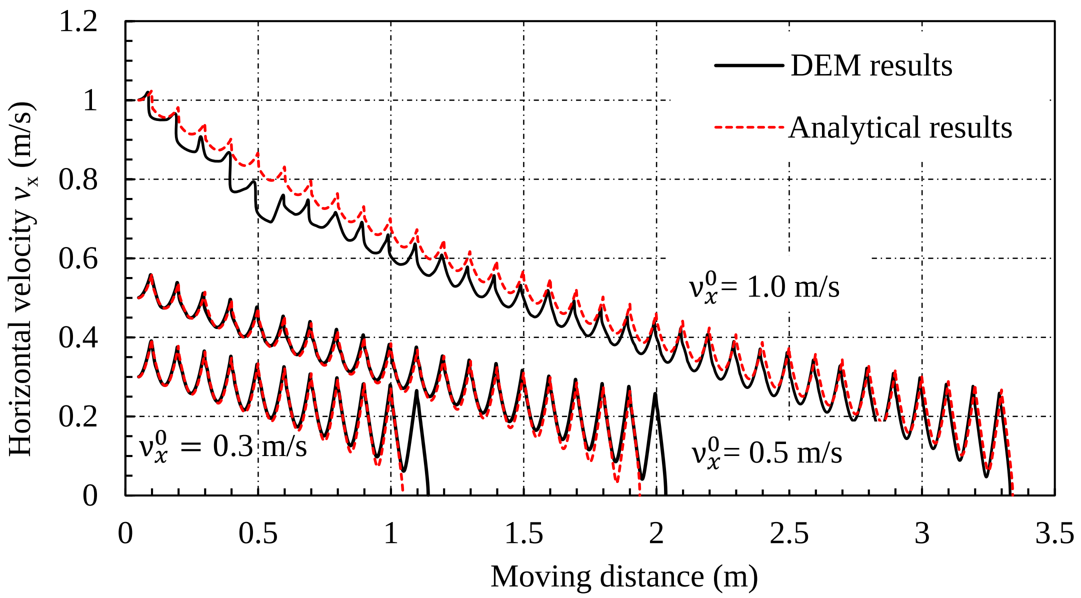

Figure 7. The results of the horizontal velocity versus the distance obtained for the disc assigned three different initial velocities v_x^0 to travel on the same substrate as specified on Figure 1 where the moving disc radius is r= 0.3 m, base discs radius is r_j=0.05 m, and damping β_n = 0.5.

In Figure 7, all three curves exhibit a 'saw-tooth' mode. This mode is caused by the bumpy surface: accelerating on down-slopes and decelerating on up-slopes. The horizontal velocity of the disc goes down at the end of the travel, as a result of energy loss at collisions. Excellent agreement is attained between the DEM results and the analytical solutions across the three cases of different initial velocities. The pairs of curves exhibit agreed amplitudes, frequencies, gradient and the final moving distances of the disc. This suggests that the DEM simulation can capture the trajectory of the disc which travels at various initial velocities, validating the capability of the DEM model to predict the loss of kinetic energy. In both the numerical and analytical scenarios, the dissipation of energy is attributed to the asperity collision along the substrate. At each collision, the velocity reduced at a gradient of 0.013 m/s per disc or 0.25 m/s per meter. It is noted that the numerical predictions deviated from the exact results at the early stage of travel if v_x^0 increased from 0.5 to 1.0 m/s. The velocity discrepancy at the early stage arises from the conditions assumed for the DEM and analytical methods respectively. As opposed to the analytical method, DEM assumes occurrence of particle–surface overlaps in collisions. It means that part of kinetic energy is converted to the elastic potential energy. Where the overlaps are relatively significant, i.e., at the early stage of greater velocity, greater energy conversion occurs and the kinetic energy and the corresponding velocity become less. The total mechanical energy however remains the same, which explains that the curves eventually agree where the velocity reduces and the overlaps become less significant.

4. Simulation Results

The validated DEM model was used to perform a parametric study. The study was focused on the travel mode of the disc of interest where important material properties and surface asperity characteristics were changed. The properties included the material damping, collision angle and mixed asperities surface. In addition, the energy transformation associated with the disc travel in each of the simulation cases was examined.

4.1 Damping

Damping influences the energy loss at collision. To gain an insight into the influence, the DEM model was applied to the discs assigned two damping coefficients, β_n = 0.1 and 0.9, respectively. The moving disc was assigned an initial velocity of v_x^0=0.5 m/s. The rest conditions remained the same as for the model used in the validation section. The simulation results, in the form of the velocity versus the moving distance curves, are provided in Figure 8. As shown in Figure 8 (a) and (c), close agreement is obtained between the DEM and analytical results obtained for the two cases β_n = 0.1 and 0.9. In both cases, the moving discs travel through 19 base discs and stops on the trough between the 19th and 20th discs. This agreement suggests that the damping coefficient less likely influenced the mode of overall energy dissipation of the moving disc, where the other conditions remained the same. However, the energy dissipation at each collision can be different, as shown in Figure 8 (b) and (d). These two figures present the velocity versus distance relationship for disc *M* travelling through the first three base discs. When the damping coefficient was relatively small (Figure 8 (b)), two collisions, as represented by the corresponding vertical short lines, and one bounce, as of the short horizontal short line, occurred. When the damping coefficient increased as in Figure 8 (d), one collision (and no bounce), as of the short vertical line, occurred. Disc *M* was in the motion of sliding for the rest part of the travel on the same base disc. For both cases, the moving disc eventually losed the normal velocity when it contacted the base asperity. For example, in Figure 1, the moving disc finally slide at the surface of base disc *j*+1, no matter of the collisions number, and the only change to the moving disc was its normal velocity. This explains that the damping coefficient does not affect the actual trajectory of disc on the surface, and the energy dissipation is greatly influenced in a single collision (Figure 8 (b) and (d)).

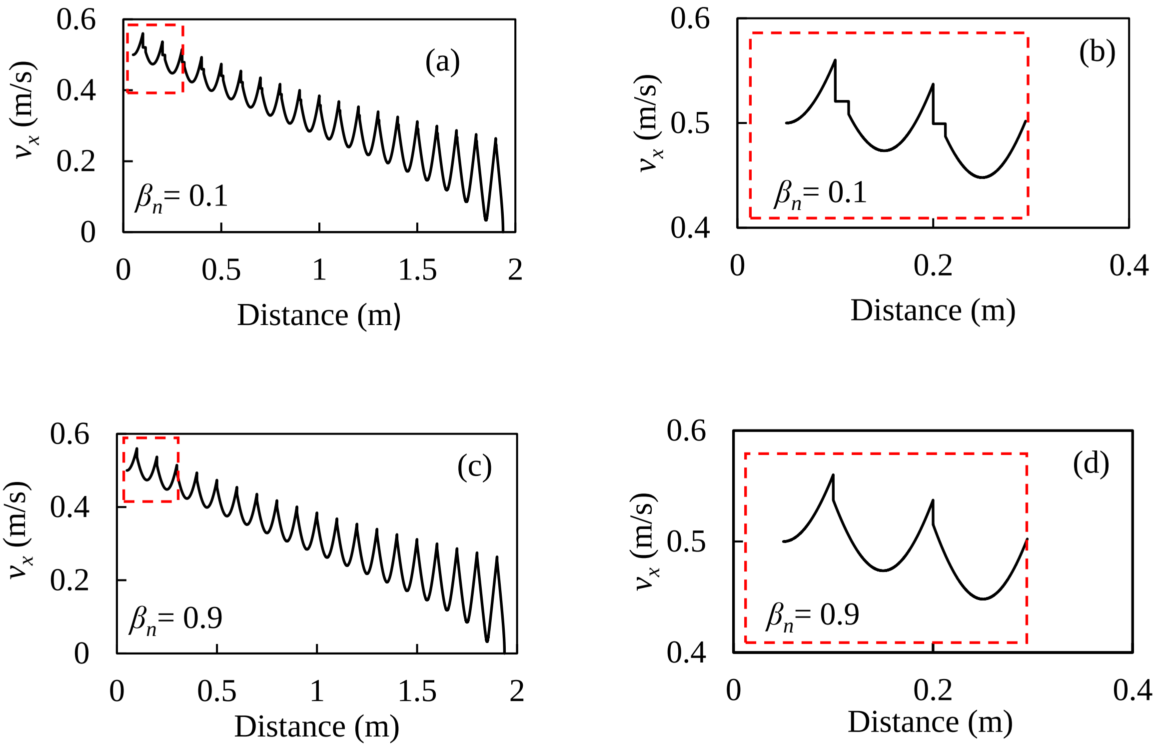

Figure 8. The results of the horizontal velocity v_x versus the moving distance obtained for the disc traveling on the substrate model as specified on Figure 1 where the moving disc radius is r= 0.3 m and the base discs radius is r_j=0.05 m, under different damping conditions: (a) damping β_n= 0.1, the complete travel profile; (b) β_n= 0.1, the travel profile through the first 3 discs; (c) damping β_n= 0.9, the complete travel profile; and (d) β_n= 0.9, the travel profile through the first 3 discs.

4.2 Loss of energy at different damping conditions

To gain a further insight into the effect of damping on the travel mode of the disc, energy dissipation developed in different damping conditions was examined. The DEM model was applied to asperity surfaces assigned six different damping coefficients β_n = 0.1, 0.2, 0.3, 0.4, 0.5, and 0.9 respectively. The initial velocity of the disc was v_x^0=0.5 m/s, whereas the rest conditions remained the same as in the validation study. In order to quantify the loss of energy at each collision, we defined the following equation:

$$\Delta E_{\beta,j} = -(E_{m,j} - E_{m,j-1}) \tag{39}$$

where $\Delta E_{\beta,j}$ is the energy dissipated at the base disc j; $E_{m,j}$ and $E_{m,j-1}$ are the system mechanical energy measured when the moving disc is in contact with base disc j and $j-1$, respectively. The mechanical energy of the system can be calculated as:

$$E_m = E_k + E_s + U \tag{40}$$

where E_k, E_s and U are the kinetic energy, strain energy at contact, and gravity potential, respectively, and are calculated using corresponding energy expressions. The gravity potential takes the initial elevation as the reference. Energy dissipation at the first collision between the moving disc and a new substrate asperity is of particular interest, because it denotes the primary collision while the remaining bounces are categorised as secondary collisions.

The relationships of energy loss at each primary collision versus distance for the discs assigned different damping coefficients are provided in Figure 9. In all cases, the energy dissipation rate (i.e., the curve gradient) decreased with the distance. This is because the slower the particle was moving, the less the kinetic energy was dissipated. However, the proportion of energy dissipation was noticeably different between $\beta_n = 0.1$ and 0.9 in each collision. On a lower damping coefficient (i.e., $\beta_n = 0.1$), multiple collisions occurred at each base substrate, and the energy loss in the primary collision used only a proportion of the total energy which is represented by the solid line in Figure 9. In comparison, when β_n increased to 0.9, the loss of primary energy was nearly equal to the loss of total energy. Despite the variation of energy dissipation in primary collisions, similar trendlines of the total energy loss were identified across the cases examined. As explained in the model development section, the total energy loss at each base disc is dependent on the normal velocity when the moving disc first contacts a new base disc. Figure 9 also suggests that asperity-induced energy loss was velocity-dependent, which resulted in viscous behaviour.

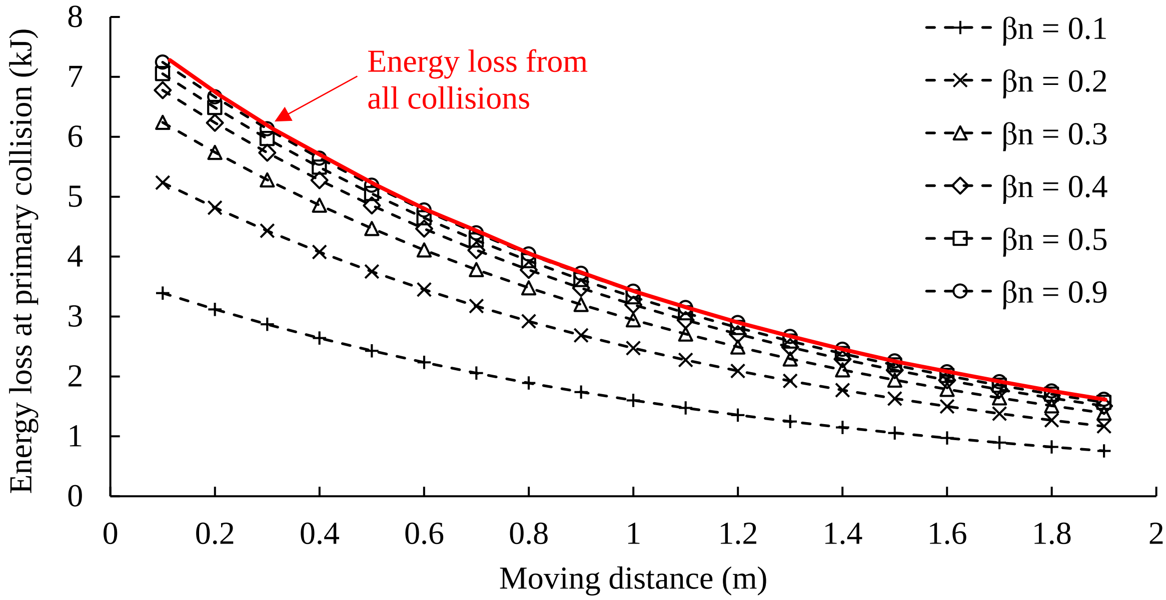

Figure 9. The results of the energy loss at the primary collision versus the moving distance obtained for the disc traveling on the substrate model as specified on Figure 1 where the moving disc radius is r= 0.3 m and the base discs radius is r_j=0.05 m, under different damping conditions.

4.3 Energy transformation

This section further examines the energy transformation occurred when the disc moves on the asperity surface. The total energy of the system E_t contains two parts: the mechanical energy E_m and dashpot energy E_β. The relationship is expressed as:

$$E_t = E_m + E_\beta \tag{41}$$

Apply the above relationship to the case of β_n = 0.9 and v_x^0 =1.0 m/s. The total energy and the energy components versus disc moving distance are plotted in Figure 10. At the initial position, the dashpot energy and strain energy were zero. Since the moving disc was placed at the crest of the base asperity, the sum of the gravity potential and kinetic energy was in peak. With an increase in the moving distance, a portion of the kinetic energy and gravity potential was transformed to the strain energy, while the rest portion was dissipated at collisions, in the form of heat and sound. It is clear that the loss of kinetic energy was equal to the increase of dashpot energy, because the total energy was constant throughout the kinetic process. Where the horizontal velocity decreased to a small value to slide over the last disc, the moving disc bounced, back and forth, in the trough of the last two base discs until the kinetic energy was dissipated completely. Figure 10 also shows the contribution of contact overlap to the energy transformation, as captured by strain energy E_s. When the velocity reduced at the later stage of travel, the influence of contact overlap became less significant. The strain energy was nearly zero after the moving disc travels to 0.5 m.

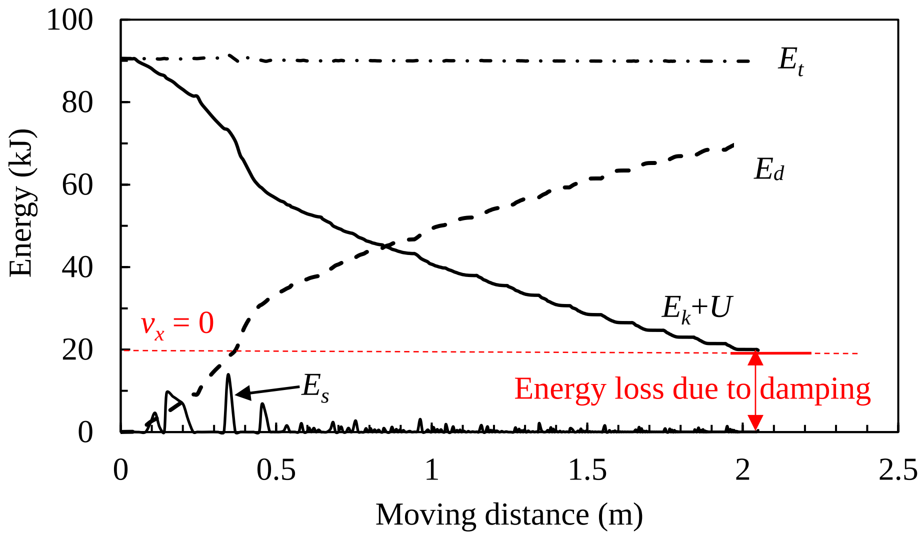

Figure 10. The results of the energy components and dissipation versus the moving distance obtained for the disc traveling on the substrate model as specified on Figure 1 where the moving disc radius is r= 0.3 m, initial velocity is v_x^0 =1.0 m/s, base discs radius is r_j=0.05 m, and damping is β_n = 0.9.

4.4 Surface asperity gap

The previous sections confirm that surface asperity can influence trajectory of moving object. According to [16], however, the bumpy surface can be described as a collection of different asperities (e.g., varying amplitudes). It is worth assessing characteristics of surface asperity and examining how the characteristics influence travel of disc. For example, it is still not clear about the relationship between the asperity amplitude parameters and energy dissipation, such as whether it is linearly related to energy loss or not. In this section, the asperity properties, including the average asperity and asperity variance, are evaluated against the energy loss.

There are a number of different methods that can be used to constitute the roughness degrees of the substrate. Gadelmawla et al. [29] suggested the use of asperity amplitude parameters. Specifically, one of the basic properties used to describe a rough surface is R_a, the average of the absolute values of the profile height deviation from the mean line that is recorded with the elevation length. This method is complicated and subject to the determination of the mean line. As a further step to the approach illustrated on Figure 1, a simplified approach was developed in the current study. The concept was to constitute the surface asperity using a set of discs with the same radius $\bar{r}$ which were spaced per $\eta \times \bar{r}$ where η is the gap coefficient. In this study, the radius $\bar{r}$ ranged from 0.04 to 0.07 m, and η from 0 to 1. The model developed based on the disc gaps is illustrated in Figure 11. The average asperity per distance, $\bar{y}$, is expressed as:

$$\bar{y} = \frac{\int_0^{\bar{r}\times(1+0.5\eta)} y\,\mathrm{d}y}{\bar{r}\times(1+0.5\eta)},\ y\in\left[0,\bar{r}\times(1+0.5\eta)\right] \tag{42}$$

The variance of the asperity is expressed as:

$$\mathrm{Var}(y) = \frac{\int_0^{\bar{r}\times(1+0.5\eta)} (y-\bar{y})^2\,\mathrm{d}y}{\bar{r}\times(1+0.5\eta)},\ y\in\left[0,\bar{r}\times(1+0.5\eta)\right] \tag{43}$$

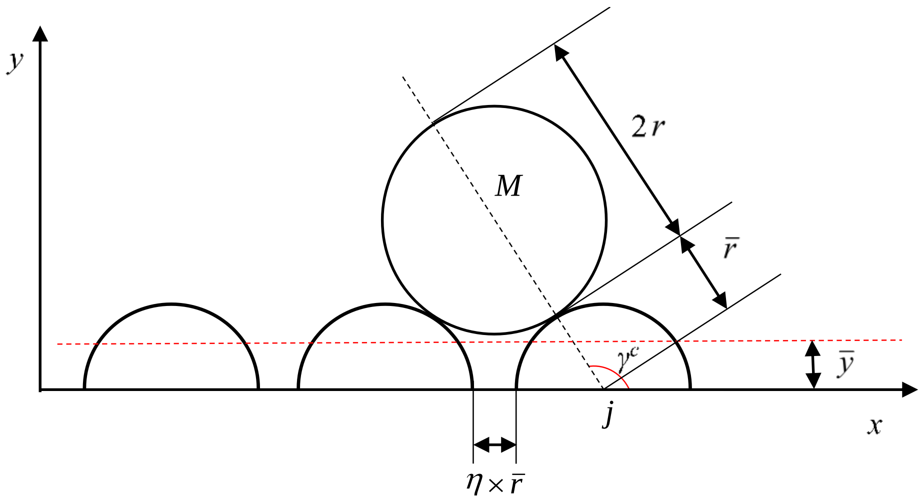

Figure 11. The asperity model developed based on gap coefficient η and average disc radius $\bar{r}$ which determines $\bar{y}$, the average asperity per distance.

Simulations were performed based on the model shown in Figure 11. The simulations were focused on the disc travel distance versus asperity characteristics, including the average asperity elevation and asperity variance. These characteristics were examined by considering the base disc radii, disc gaps and asperity average elevation. The rest simulation conditions remained the same as in the validation section. A total of 44 simulations were performed to collect the disc travel distance information and were plotted against surface average height or height variance. The simulation results are provided in Figure 12 and Figure 13 respectively.

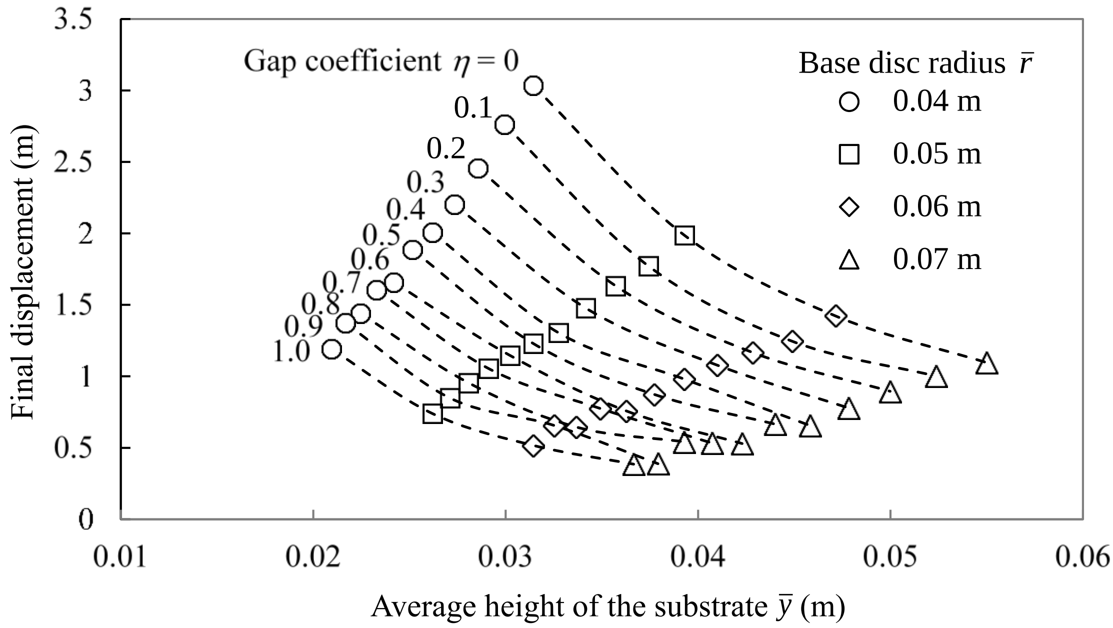

Figure 12. The results of the final displacement versus the average height of the substrate $\bar{y}$ obtained for the disc traveling on the substrate model as specified on Figure 11 where the moving disc radius is r= 0.3 m, initial velocity is v_x^0 =1.0 m/s, and damping is β_n = 0.9, with different base disc radii $\bar{r}$ and gap coefficients η.

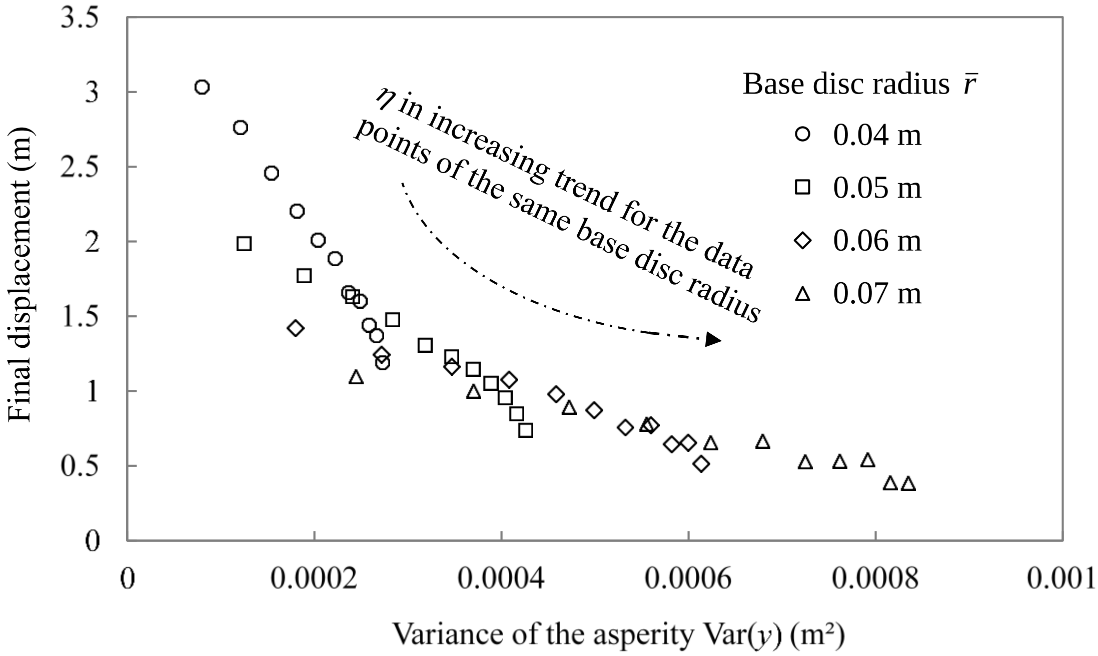

Figure 13. The results of the final displacement versus the variance of the asperity Var(y) obtained for the disc traveling on the substrate model as specified on Figure 11 where the moving disc radius is r= 0.3 m, initial velocity is v_x^0 =1.0 m/s, and damping is β_n = 0.9, with different base disc radii $\bar{r}$ and gap coefficients η.

In Figure 12, the final displacement of the moving disc is plot per the base disc radius $\bar{r}$ and gap coefficient η. With the same gap coefficient, the asperity average height increased with the disc radius, resulting in a decrease of in the final displacement. When the disc radius remained constant, an increase in the gap ratio decreased the substrate height, which in turn decreased the final displacement. However, the final displacement was independent on the average height of the surface substrate, because the actual maximum displacement occurred at an intermediate surface height (e.g., the case with $\bar{r}$ = 0.04 m and η = 0). This indicates that the average surface height was not linearly related to the trajectory of the disc. In comparison, the surface-height variance provides better quantification of final displacement. It can be identified that the lower the asperity-height variance was, the farther the object can travel. Theoretically, the asperity gap helps refine surface asperity characteristics. However, there are still some slight overlaps between different groups of radii as shown in Figure 12–13, and these points inside the overlap area produce a reverse trend as opposed to the general relationship. Hence, it is necessary to seek additional description of surface roughness which is discussed in the following section.

4.5 Collision angle

In this section, the collision angle γ^c is used to characterise surface roughness. At each collision, the collision angle influences the loss of the normal velocity of the moving disc as shown in Figure 8. The collision angle γ^c is different from the contact angle γ. The collision angle γ^c is defined as the contacting angle when the moving disc collides a new base disc and, as shown in Figure 11, is calculated as:

$$\gamma^c = \arccos\frac{\bar{r}\times(1+0.5\eta)}{r+\bar{r}},\ \gamma^c \in\left[\frac{\pi}{2},\pi\right] \tag{44}$$

It should be noted that there may be other collisions occurred between the moving disc and the base disc of interest. However, due to a relatively low horizontal velocity, the collision must happen in the middle of the two base discs where most of the kinetic energy is dissipated, as shown in Figure 9.

The final displacements are plotted against the collision angle γ^c as shown in Figure 14. A monotonic relationship was observed: the smaller the collision angle was, the less distance the disc can move on the surface. The final displacement was entirely dependent on the collision angle. From this perspective, the collision angle was a parameter governing the surface roughness.

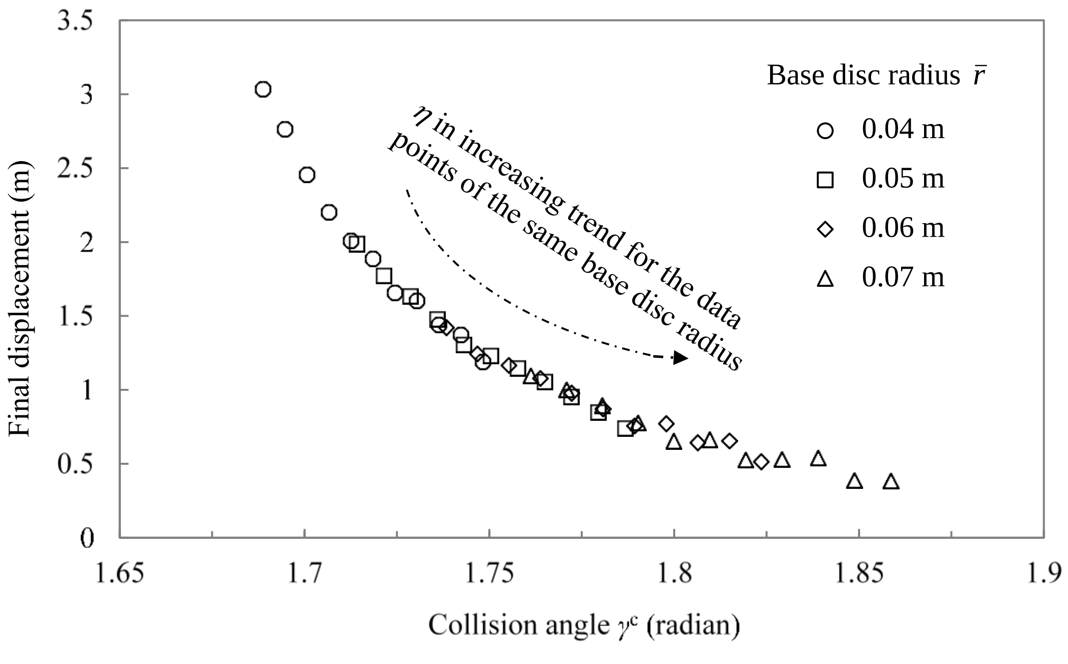

Figure 14. The results of the final displacement versus the collision angle γ^c obtained for the disc traveling on the substrate model as specified on Figure 11 where the moving disc radius

is r= 0.3 m, initial velocity is v_x^0 =1.0 m/s, and damping is β_n = 0.9, with different base disc radii $\bar{r}$ and gap coefficients η.

4.6 Mixed asperities

A surface of even asperity facilitates model development and simulation. However, a surface of mixed asperities often occurs. To account for the mixed asperities, the substrate was constituted with a group of discs of different radius r_j and gap coefficients η. The schematic is shown in Figure 15. The two governing parameters r_j and η were assumed to be independent and, as per Persson et al. [8], follows a normal distribution, N (μ, σ), where μ is the mean and σ is the standard deviation. The two distribution parameters are determined in terms of the disc travel distance expected. The distance travelled under the mixed asperities varies significantly, but, due to the presence of varying collision angles arising from the mixed asperities, is relatively less than that obtained in the even asperity cases. In order to properly measure the actual collision angle, a threshold distance of passing over 20 base discs was specified. To satisfy the distance, we iterated the distributions for the radii and gaps in terms of the initial velocity, and determined the corresponding distributions as N (40, 10) and N (20, 6.5) respectively. The distribution details are provided in Figure 16 and Figure 17 respectively.

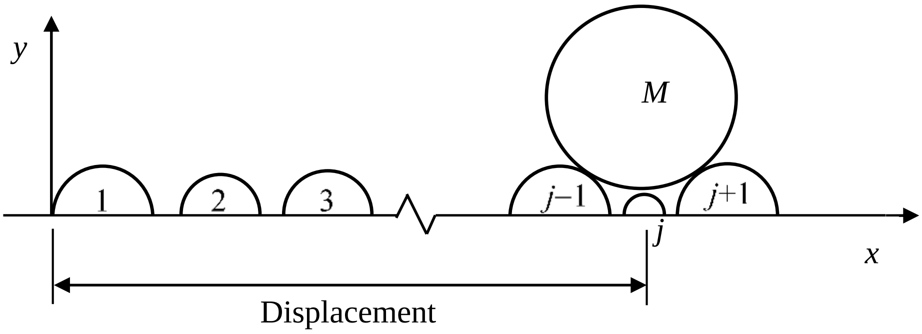

Figure 15. The asperity model developed based on mixed surface asperities which vary in the base discs diameter and gaps.

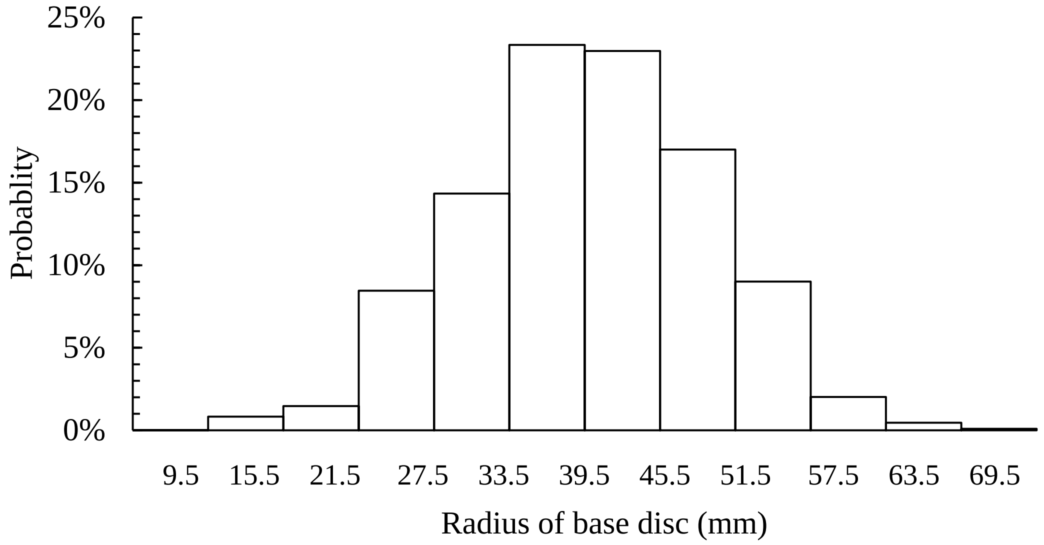

Figure 16. The normal distribution of base disc radii used for the model provided on Figure 15.

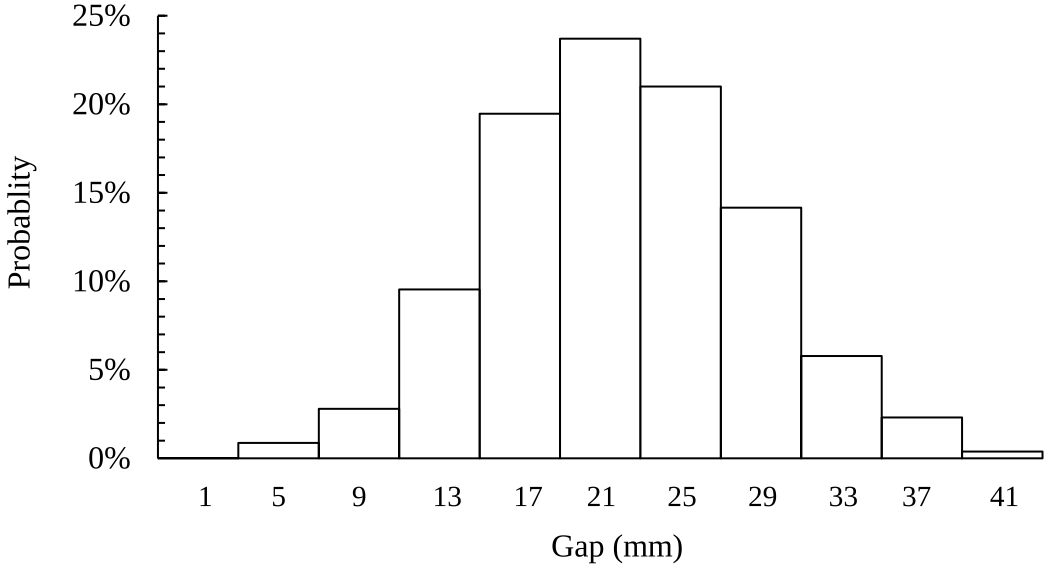

Figure 17. The normal distribution of base disc gaps used for the model provided on Figure 15.

Additional efforts were made to gauge the actual collision angle. In the case of mixed asperities, the actual collision angle cannot be determined before the disc rest, as opposed to the even asperity case. For example, Figure 15 shows that the moving disc does not contact the base disc j. Therefore the collision angle between the moving disc and the substrate j does not have physical meaning. Also, due to the complexity of the substrate, the moving disc may exhibit some significant jumps depending on its initial velocity. For these reasons, the actual trajectory of the moving disc was gauged to attain the actual collision angles.

In order to validate the surface properties of energy dissipation for an actual bumpy surface, a sufficient number of different surfaces where asperities are randomly distributed need to be generated. This collection of substrates can be generated in *PFC2D* by using a random number, called 'seed', which governs particles generation. Changing this 'seed' value can generate different assemblies of the discs and thus the substrates which we followed to reproduce a collection of surfaces of mixed asperities. We generated a total of 250 sample surfaces and flew a disc, at an initial velocity v_x^0 = 0.5 m/s, through each of the surfaces. The relationship between the dissipated energy and collision angle is presented in Figure 18. The dissipated energy occurred at the 15^{th} collision with respect to the actual average collision angle was calculated. At the assigned velocity, the moving disc passed through more than 20 base discs, but the number of the effective collisions as presented in Figure 18 was less, as some base discs, e.g., the *j*th particle as shown in Figure 15, were of low elevation and not in contact with the moving disc.

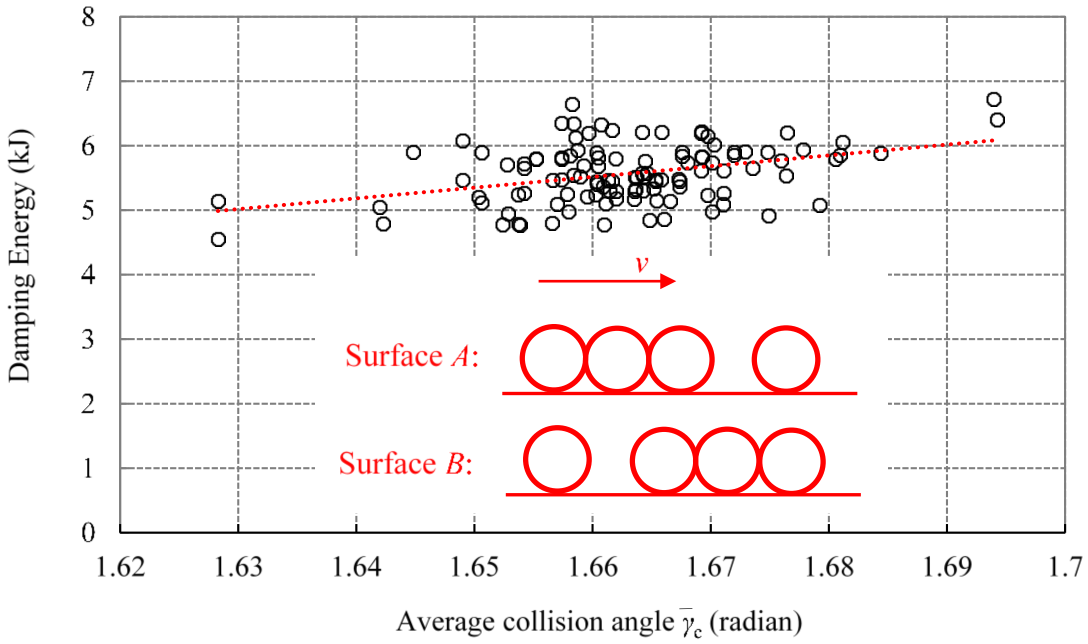

Figure 18. The results of the dissipated energy at the 15th collision versus the actual average collision angle $\bar{\gamma}^c$ obtained for the disc traveling on the substrate model as specified on Figure 15 where the discs radius and gaps are randomly generated in a total of 250 samples.

In Figure 18, the average collision angle $\bar{\gamma}^c$ was calculated as the sum of the collision angles divided by the number of collisions. As can be seen, the dissipated energy increased with the increase of the average collision angle, which generated a linear distribution. However, the spread of data suggests a results variation. The variation arises from the varying surfaces tested, which influences the energy dissipation. For example, surfaces *A* and *B* may exhibit identical substrate properties, e.g., the same collision angle, average height and height variance, but differ in sequences of elements (e.g., the location of gap) and therefore yield different energy dissipation modes. With respect to the energy dissipation, the mode for the disc on the surface of mixed asperity differed from that on the surface of even asperity. On the even asperity surface, the kinetic energy was gradually damped at each collision, while on the mixed asperity surface the kinetic energy was dissipated in a fluctuating pattern, greater or less, depending on the gaps and discs size to collide with. Sometimes significant energy was dissipated completely simply because of collisions with the next relatively larger gap or disc on the surface. These odd asperities often bring up a relatively greater collision angle and those posing the maximum collision angle are worth further examining.

4.7 Maximum collision angle

Theoretically, the moving disc can rest at any trough on a bumpy surface, but the simulations suggest that the disc often rests at the trough where the maximum collision angle occurs. The probability of the coincidence can be obtained by examining the relationship between the at-rest distance and the location of trough that the maximum collision angle occurs. The location of trough is represented by the normalised distance, L_r, which is expressed as:

$$L_r = \frac{S_{r,\max}}{S_{\text{stop}}},\ L_r \in [0,1] \tag{45}$$

where $S_{\gamma,\max}$ is the position corresponding to the maximum collision angle, and S_{stop} is the total moving distance. If $L_r = 1$, the position for the maximum collision angle coincides with the total distance. Otherwise, the maximum collision angle occurs before the disc is at rest.

Of the 250 surfaces tested, the probability for L_r is plotted in Figure 19. Approximate 65% surfaces had the discs rest at the troughs of the maximum collision angle, suggesting occurrences of instant stop. The discs in the remaining tests passed through the troughs of the maximum collision angle and travelled farther. The additional distances the discs travelled was independent on the locations of the troughs of the maximum collision angle, due to the even probability for $L_r = 0$ to 0.9. The probability distribution is explained in terms of at least three factors: *i*) the kinetic energy to overcome the collision angle, *ii*) the locations where the maximum collision angle occur, and *iii*) the initial velocity of the disc. Greatest kinetic energy is required to pass by the trough of the maximum collision angle. This trough prohibits the disc to move farther if the energy fails to meet the threshold required to pass by. The threshold applies to a greater number of discs than those raised by less ‘tough troughs, and therefore builds to greater occurrences of discs at rest. The kinetic energy has not been dissipated significantly at the early stage of travel and likely enables the disc to pass over the trough of the maximum collision angle that occurs. The opposite takes place at the mid- to late stages of travel where the energy has been dissipated down to a lower level. Meanwhile the initial velocity should fall into a range so that the kinetic energy is properly loaded and dissipated over the mixed asperities.

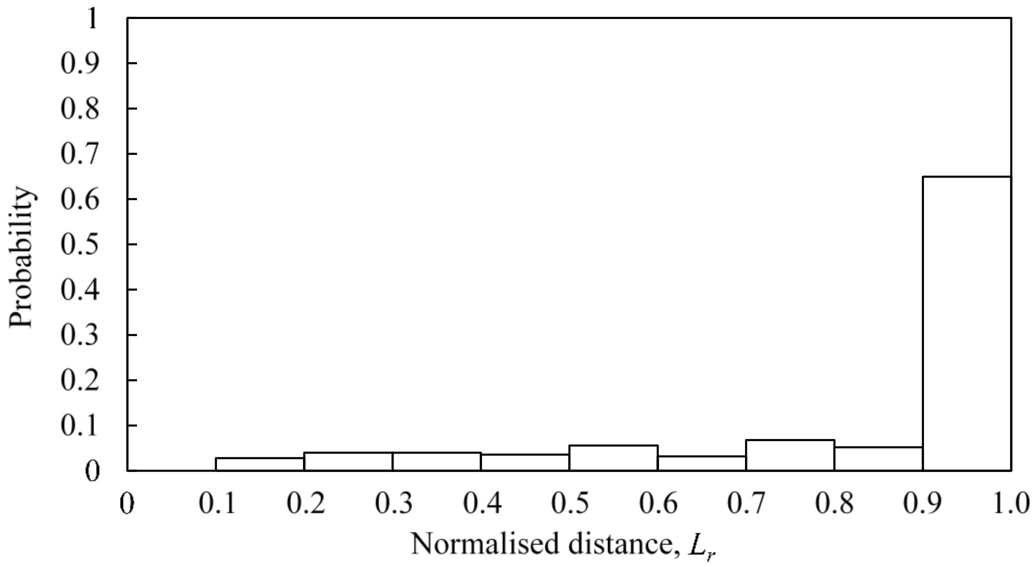

Figure 19. The probability for the normalised distance L_r obtained for the disc that travels on the substrate model as specified on Figure 15 where the discs radius and gaps are randomly generated in a total of 250 samples.

4.8 Asperity and sub-asperity mixed surface

In sections 4.1–4.7, we have examined the trajectory of the moving disc travelling on an asperity surface. However, on a real surface, there are sub-asperities affixed over the primary surface which influences the trajectory and energy loss of the moving disc. To account for the surface sub-asperities, we constituted a surface mixed with primary and sub-asperities. To attain the mixed surface, clumps of discs were used. The clump models are provided in Figure

20. Clump *A* was spherical. Clumps *B* and *C* exhibited different sub-asperities. The sub-asperities were formed by affixing a set of discs together, each disc sharing a section of the circular perimeter. The equivalent radius of clumps *B* and *C* was equal to the radius of clump *A*. If travelling on the asperity and sub-asperity mixed surface, the moving disc is subjected to greater collisions than on the asperity surface, and the additional collisions are expected to cause greater energy loss in a shorter distance. Similar asperity and sub-asperity mixed surface can occur to the moving disc, which prompts the importance of simulations.

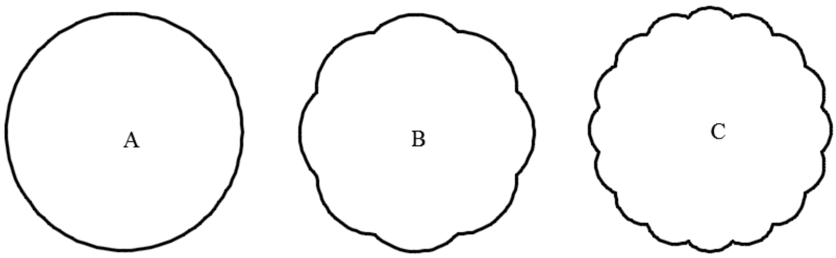

Figure 20. The clumps used to represent primary and sub-asperities: clump *A* has primary asperity, clump *B* combines primary asperity and 8 equal sub-asperities, and clump *C* combines primary asperity and 16 equal sub-asperities.

Clumps *A*, *B* and *C* were paired to reproduce the moving disc and base discs. Use number '1' to denote the moving disc and number '2' to the base discs for the substrate. For example, the combination *A*1*B*2 represents the model of the clump *A*-based disc moving on the clump *B*-based substrate. In simulations, we designed four combinations: *A*1*A*2, *A*1*B*2, *B*1*B*2 and *C*1*B*2, in the order of increasing number of asperities. The moving disc of the last three models was initially placed in the trough of interest, thus enabling a stable start. The properties of the clumps, such as the damping coefficient, density, volume and contact stiffness, remained the same as in the validation case. The moving disc was assigned an initial horizontal velocity of v_x^0 =0.5 m/s. Note that, for a clump of discs, the discs collided eccentrically, leading to a residual rolling velocity. In the simulations, rolling was restricted for the last three models to create the same condition with the first model. The simulation results are provided in Figure 21. The figure shows the relationship between the horizontal velocity and moving distance captured for the four models.

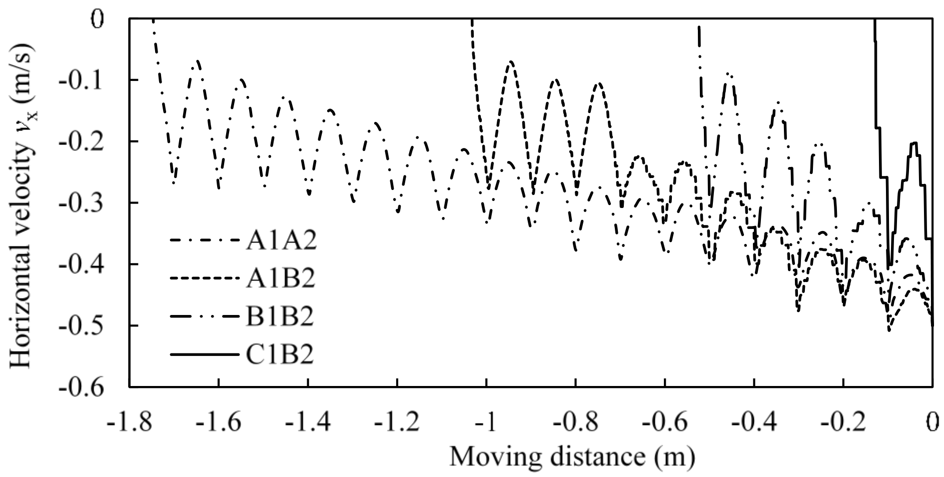

Figure 21. The results of the horizontal velocity v_x versus the moving distance obtained for the disc traveling on the substrate model as specified on Figure 1 where the moving and base discs use clumps defined on Figure 20, the moving disc is assigned an initial velocity v_x^0 =0.5 m/s, and the damping is β_n = 0.9.

In Figure 21, when the number of the surface sub-asperities increased, the moving disc travelled a shorter distance. For example, model *C*1*B*2 travelled around one-tenth of the distance attained by model *A*1*A*2. It is suggested that the sub-asperity exhibited a significant effect on the final displacement. At the surface of a primary asperity, the sub-asperities increased the number of effective collisions. At the same distance, greater energy was dissipated in model *C*1*B*2 than in the other models of fewer sub-asperities. In addition, the sub-asperities on the base discs caused a lower collision angle and thus greater energy dissipation.

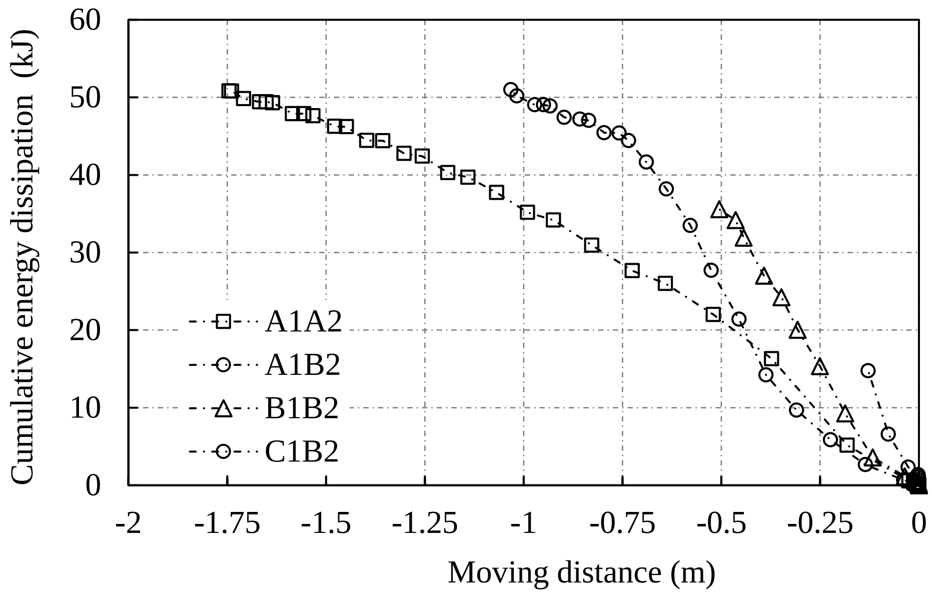

Figure 22. The results of the cumulative energy dissipation versus the moving distance obtained for the disc traveling on the substrate model as specified on Figure 1 where the moving and base discs use clumps defined on Figure 20, the moving disc is assigned an initial velocity v_x^0 =0.5 m/s, and the damping is β_n = 0.9.

The simulations performed in this study suggested that surface asperity-induced friction can be considered as a larger number of individual collisions, and that these collisions cause the dissipation of kinetic energy. One of the major differences between the two conceptions (the friction vs. the collision) is that the collision-induced energy loss is velocity-dependent, as shown in Figure 8, while the friction conception assumes that the friction force is independent on the velocity of the moving object. The collision conception agrees with earlier studies performed at an atomic level [19,30-31]. In these studies, the friction force experienced velocity-dependent viscous behaviour. Research on atomic- or molecular-scale friction [30,32-33] also identified a sawtooth friction behaviour at the nanoscale, which is in further support of the current simulation results. This means that the surface of interest contains a large number of asperities and sub-asperities, and that the collisions at individual asperities and sub-asperities cause the surface friction attained at the macroscale.

Where the sub-asperity surface occurs, the moving disc rotates due to the eccentric force acting on the disc. In this section, the rotation of the moving disc is examined. We designed three models: *A*1*B*2, *B*1*B*2 and *C*1*B*2, where the moving disc was assigned clumps *A*, *B* and *C* respectively, and the substrate surface used clump *B* throughout. The relationship between the rolling velocity and the sliding distance is plotted in Figure 23. Define the anti-clockwise rolling to be positive. The moving disc in model *C*1*B*2 travelled a longer distance than the distance obtained in model *B*1*B*2, which was different from the results if the rolling was restricted. As shown in Figure 21, the moving disc in model *B*1*B*2 travelled much farther than the disc in model *C*1*B*2. This can be explained from the perspective of a collision impact. For model *B*1*B*2, the collision sometimes induced a negative angular velocity, and rotation at this direction prohibited its movement at the surface. The translational velocity at the contact point was therefore reduced, and the moving disc was finally at rest.

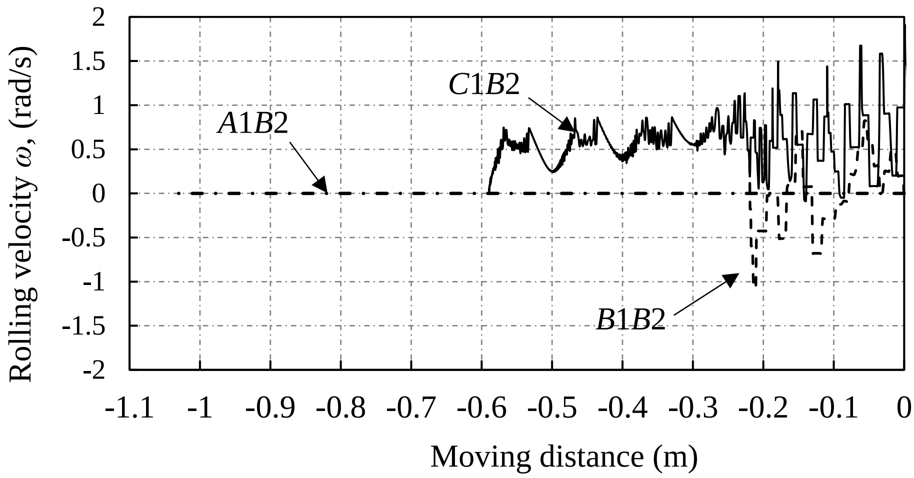

Figure 23. The results of the rolling velocity versus the moving distance obtained for the disc traveling on the substrate model as specified on Figure 1 where the moving and base discs use clumps defined on Figure 20, the moving disc is assigned an initial velocity v_x^0 =0.5 m/s, and the damping is β_n = 0.9.

5. Conclusions

This paper models the trajectory of a disc moving on a bumpy surface and examines the energy dissipation at collisions. An analytical model based on a single-contact collision conception was developed. The model was able to capture the trajectory of the moving disc. The analytical model was established and applied to validate a DEM model. The DEM model was applied to examine the effects of important surface asperity properties on the kinetic behaviour of the moving disc. The properties included the material damping, average asperity height, height variance, gaps, collision angle and sub-asperities. The energy loss associated with the property characteristics was also examined. The simulations arrived at the following conclusions.

Upon contacting, the moving disc bounced on an asperity surface several times and then slide on the same asperity surface. The first collision between the moving disc and the base disc consumed a major portion of the energy, while the energy dissipated at other bounces was marginal. The actual collision angle was in a monotonic relationship with the maximum distance of the moving disc. The collision angle outweighed the other surface properties, such as the average asperity height and surface-height variance, in respect to characterising surface roughness.

The surface sub-asperities accelerated the loss of kinetic energy. If the sub-asperities were of high density, the surface can dissipate a high level of kinetic energy. Sub-asperity-induced rolling decreased translational velocity and thus restricted the motion of the disc. The energy dissipation of the moving disc was positively proportional to the velocity of the disc. The conception of asperity-induced energy loss reflected the effects of collisions and provided an understanding of surface friction at microscale.

Acknowledgements

This study is performed under the supports provided by the Australian Research Council (project No. DP140103004) and the University of Adelaide. Professional editor, Leticia Mooney, provided copyediting and proofreading services, according to the guidelines laid out in the university-endorsed national 'Guidelines for editing research theses'.

Notations

D_j^t	relative distance between the moving disc and base disc at time step t
E_m	system mechanical energy
E_t	total energy
E_k	kinetic energy
E_β	dashpot energy loss
F_n^d, F_s^d	normal and dashpot force
F_n^h, F_s^h	nonlinear normal and shear contact force
g	gravity acceleration
k_n	normal stiffness
L_r	relative distance of the collision angle
m_1, m_2	mass of the bodies 1 and 2
m_c	mass of the system
r	radius of the moving disc
r_j	radius of base disc j
$\bar{r}$	average radius of the base disc
$S_{\gamma,\max}$	distance where the maximum collision angle occurs
S_{stop}	total moving distance
t	time step

Δt,	time step increment
Δt_0	time step increment at bounce
v	velocity
v_n	normal velocity before collision
v_s	tangential velocity before collision
$v_{n,r}$	normal velocity after collision
x^t, y^t	centre position of the moving disc at time step t
U	gravity potential
α_n	restitution coefficient
β_n	damping coefficient
γ	contact angle
γ^c	collision angle
$\bar{\gamma}^c$	average collision angle
$\dot{\delta}_n$	relative normal translational velocity
ω	angular velocity
θ	rotation angle
η	disc gap coefficient
μ	mean of normal distribution
σ	standard deviation of normal distribution

Ethical Statement

Disclosure of potential conflicts of interest: The authors declare that they have no conflict of interest.

Research involving Human Participants and/or Animals: This article does not contain any studies with human participants or animals performed by any of the authors.

Informed consent: Informed consent was obtained from all individual participants included in the study.

References

1. Yang, J., Wei, L.: Collapse of loose sand with the addition of fines: the role of particle shape. Géotechnique **62**(12), 1111-1125 (2012).
2. Jensen, R.P., Edil, T.B., Bosscher, P.J., Plesha, M.E., Kahla, N.B.: Effect of particle shape on interface behavior of DEM-simulated granular materials. International Journal of Geomechanics **1**(1), 1-19 (2001).
3. Dai, B.B., Yang, J., Zhou, C.Y.: Observed effects of interparticle friction and particle size on shear behavior of granular materials. International Journal of Geomechanics **16**(1), 04015011 (2015).
4. Doménech-Carbó, A.: On the independence of friction and restitution: an operational approach. Granular Matter **18**(1), 9 (2016).
5. Zhai, C.P., Hanaor, D., Gan, Y.X.: Contact stiffness of multiscale surfaces by truncation analysis. Int J Mech Sci **131**, 305-316 (2017). doi:10.1016/j.ijmecsci.2017.07.018
6. Holmberg, K., Ronkainen, H., Laukkanen, A., Wallin, K.: Friction and wear of coated surfaces - scales, modelling and simulation of tribomechanisms. Surface and Coatings Technology **202**(4-7), 1034-1049 (2007). doi:10.1016/j.surfcoat.2007.07.105
7. Majumdar, A., Tien, C.L.: Fractal characterization and simulation of rough surfaces. Wear **136**(2), 313-327 (1990). doi:10.1016/0043-1648(90)90154-3

8. Persson, B.N.J., Albohr, O., Tartaglino, U., Volokitin, A.I., Tosatti, E.: On the nature of surface roughness with application to contact mechanics, sealing, rubber friction and adhesion. J Phys-Condens Mat **17**(1), R1-R62 (2005). doi:10.1088/0953-8984/17/1/R01

9. Buckley, D.H.: Surface Effects in Adhesion, Friction, Wear, and Lubrication, vol. 5. Elsevier, (1981)

10. Tayebi, N., Polycarpou, A.A.: Modeling the effect of skewness and kurtosis on the static friction coefficient of rough surfaces. Tribology International **37**(6), 491-505 (2004).

11. Svahn, F., Kassman-Rudolphi, Å., Wallen, E.: The influence of surface roughness on friction and wear of machine element coatings. Wear **254**(11), 1092-1098 (2003).

12. Zappone, B., Rosenberg, K.J., Israelachvili, J.: Role of nanometer roughness on the adhesion and friction of a rough polymer surface and a molecularly smooth mica surface. Tribology Letters **26**(3), 191 (2007).

13. Jensen, R.P., Bosscher, P.J., Plesha, M.E., Edil, T.B.: DEM simulation of granular media—structure interface: effects of surface roughness and particle shape. International Journal for Numerical and Analytical Methods in Geomechanics **23**(6), 531-547 (1999).

14. Dippel, S., Batrouni, G., Wolf, D.: Collision-induced friction in the motion of a single particle on a bumpy inclined line. Physical Review E **54**(6), 6845 (1996).

15. Jenkins, J.T.: Boundary conditions for plane flows of smooth, nearly elastic, circular disks. Journal of Fluid Mechanics **171**, 53-69 (1986). doi:10.1017/S0022112086001362

16. Greenwood, J., Williamson, J.: Contact of nominally flat surfaces. Proceedings of the Royal Society of London A: Mathematical, Physical and Engineering Sciences **295**(1442), 300-319 (1966).

17. Batrouni, G., Dippel, S., Samson, L.: Stochastic model for the motion of a particle on an inclined rough plane and the onset of viscous friction. Physical Review E **53**(6), 6496 (1996).

18. Henrique, C., Aguirre, M., Calvo, A., Ippolito, I., Dippel, S., Batrouni, G., Bideau, D.: Energy dissipation and trapping of particles moving on a rough surface. Physical Review E **57**(4), 4743 (1998).

19. Valance, A., Bideau, D.: Dynamics of a ball bouncing on a rough inclined line. Physical Review E **57**(2), 1886 (1998).

20. Gollin, D., Berzi, D., Bowman, E.T.: Extended kinetic theory applied to inclined granular flows: Role of boundaries. Granular Matter **19**(3), 56 (2017).

21. Cundall, P.: Computer simulations of dense sphere assemblies. Micromechanics of Granular Materials (1988).

22. Wang, C., Deng, A., Taheri, A.: Three-dimensional discrete element modeling of direct shear test for granular rubber-sand. Comput Geotech **97**, 204-216 (2018). doi:10.1016/j.compgeo.2018.01.014

23. Mindlin, R.D., Deresiewicz, H.: Elastic spheres in contact under varying oblique forces. Journal of Applied Mechanics **20**, 327-344 (1953).

24. Itasca: PFC2D 5.0 User Manual. In. Minneapolis, MN USA, (2017)

25. Cundall, P.A., Strack, O.D.: A discrete numerical model for granular assemblies. Géotechnique **29**(1), 47-65 (1979).

26. Becker, V., Schwager, T., Pöschel, T.: Coefficient of tangential restitution for the linear dashpot model. Physical Review E **77**(1), 011304 (2008).

27. Ling, F.: Normal impact model of rough surfaces. Journal of Tribology **114**(3), 439-447 (1992).

28. Kawaguchi, T., Tanaka, T., Tsuji, Y.: Numerical simulation of fluidized bed using the discrete element method (the case of spouting bed). Transactions of the Japan Society of Mechanical Engineers Series B **58**(551), 79-85 (1992).

29. Gadelmawla, E., Koura, M., Maksoud, T., Elewa, I., Soliman, H.: Roughness parameters. Journal of Materials Processing Technology **123**(1), 133-145 (2002).

30. Gnecco, E., Bennewitz, R., Gyalog, T., Loppacher, C., Bammerlin, M., Meyer, E., Güntherodt, H.-J.: Velocity dependence of atomic friction. Physical Review Letters **84**(6), 1172 (2000).

31. Bhushan, B., Israelachvili, J.N., Landman, U.: Nanotribology: Friction, wear and lubrication at the atomic scale. Nature **374**(6523), 607-616 (1995). doi:10.1038/374607a0

32. Fujisawa, S., Kishi, E., Sugawara, Y., Morita, S.: Atomic-scale friction observed with a two-dimensional frictional-force microscope. Physical Review B **51**(12), 7849 (1995).

33. Hanaor, D.A.H., Gan, Y.X., Einav, I.: Static friction at fractal interfaces. Tribology International **93**, 229-238 (2016). doi:10.1016/j.triboint.2015.09.016